Cyanide Binding to Hexacoordinate Cyanobacterial Hemoglobins: Hydrogen-Bonding Network and Heme Pocket Rearrangement in Ferric H117A *Synechocystis* Hemoglobin†

B. Christie Vu, Henry J. Nothnagel, David A. Vuletich, Christopher J. Falzone, and Juliette T. J. Lecomte*

Department of Chemistry, The Pennsylvania State University, University Park, Pennsylvania 16802

Received June 18, 2004; Revised Manuscript Received July 23, 2004

ABSTRACT: The truncated hemoglobin (Hb) from the cyanobacterium *Synechocystis* sp. PCC 6803 is a bis-histidyl hexacoordinate complex in the absence of exogenous ligands. This protein can form a covalent cross-link between His117 in the H-helix and the heme 2-vinyl group. Cross-linking, the physiological importance of which has not been established, is avoided with the His117Ala substitution. In the present work, H117A Hb was used to explore exogenous ligand binding to the heme group. NMR and thermal denaturation data showed that the replacement was of little consequence to the structural and thermodynamic properties of ferric *Synechocystis* Hb. It did, however, decelerate the association of cyanide ions with the heme iron. Full complexation required hours, instead of minutes, of incubation at optical and NMR concentrations. At neutral pH and in the presence of excess cyanide, binding occurred with a first-order dependence on cyanide concentration, eliminating distal histidine decoordination as the rate-limiting step. The cyanide complex of the H117A variant was characterized for the conformational changes occurring as the histidine on the distal side, His46 (E10), was displaced. Extensive rearrangement allowed Tyr22 (B10) to insert in the heme pocket and Gln43 (E7) and Gln47 (E11) to come in contact with it. H-bond formation to the bound cyanide was identified in solution with the use of $^1H_2O/^2H_2O$ mixtures. Cyanide binding also resulted in a change in the ratio of heme orientational isomers, in a likely manifestation of heme environment reshaping. Similar observations were made with the related *Synechococcus* sp. PCC 7002 H117A Hb, except that cyanide binding was rapid in this protein. In both cases, the ^{15}N chemical shift of bound cyanide was reminiscent of that in peroxidases and the orientation of the proximal histidine was as in other truncated Hbs. The ensemble of the data provided insight into the structural cooperativity of the heme pocket scaffold and pointed to the reactive 117 site of *Synechocystis* Hb as a potential determinant of biophysical and, perhaps, functional properties.

Truncated hemoglobins (trHbs)[1] form a subfamily of *b* hemoproteins distantly related to vertebrate hemoglobins. They are found in many cyanobacteria, pathogenic bacteria, unicellular eukaryotes, and plants and are phylogenetically classified in three groups (I or trHbN, II or trHbO, and III or trHbP), which exhibit distinct constellations of amino acid in the heme-binding site and other key locations (*1*). The functions of trHbs have not been completely elucidated, but it is known that in the Fe(II) state, these proteins are generally capable of binding O_2 or other small ligands such as NO (*2*). Spectroscopic and structural data of several trHbs reveal that the stabilization of the bound O_2 is likely conveyed by an extensive network of hydrogen bonds (*1*, *3*, *4*). Central to this network is Tyr B10, a residue strictly conserved in groups II and III trHbs and highly conserved in group I trHbs, according to available primary structures. Tyr B10 is also present in numerous invertebrate globin sequences. Most trHbs display cavities and tunnels that are thought to facilitate exogenous ligand concentration and access to the heme iron (*5*−*9*). The hydrogen-bonding networks and dynamic hollows of trHbs constitute functionally important features that can be systematically explored with appropriate mutations and across species to improve the description of the relationship between structure and function (*10*, *11*).

The genomes of the non-nitrogen-fixing cyanobacteria *Synechococcus* sp. PCC 7002 (S7002) and *Synechocystis* sp. PCC 6803 (S6803) each contain a copy of a gene coding for a group I trHb (*12*, *13*). Although S7002 and S6803 Hbs exhibit a fold readily recognizable as that of a globin (*13*, *14*), these proteins have two peculiar structural features. In the "deoxy" state their heme iron adopts an endogenous hexacoordination scheme using two histidines—His46 (E10) and His70 (F8)[2]—as axial ligands (*13*, *15*, *16*). In the ferric

† Supported by National Science Foundation Grants MCB-091182 and MCB-0349409.

* Author to whom correspondence should be addressed [telephone (814) 863-1153; fax (814) 863-8403; e-mail jtl1@psu.edu].

[1] Abbreviations: *Ce*, *Chlamydomonas eugametos*; DQF-COSY, double-quantum-filtered correlated spectroscopy; Eq, equine; GlbN, cyanoglobin; Hb, hemoglobin; HMQC, heteronuclear multiple-quantum coherence; HSQC, heteronuclear single-quantum coherence; Mb, myoglobin; metMb, ferric myoglobin; NOE, nuclear Overhauser effect; NOESY, nuclear Overhauser effect spectroscopy; PPIX, protoporphyrin IX; rHb, recombinant hemoglobin; rHb-A, recombinant hemoglobin with covalently linked heme; rHbCN, recombinant ferric hemoglobin with cyanide bound; rHb-R, recombinant heme-reconstituted hemoglobin; S6803, *Synechocystis* sp. PCC 6803; S7002, *Synechococcus* sp. PCC 7002; TOCSY, totally correlated spectroscopy; TPPI, time-proportional phase incrementation; trHb, truncated hemoglobin; WATERGATE, water suppression by gradient-tailored excitation; WEFT, water elimination Fourier transform.

10.1021/bi048726l CCC: $27.50 © 2004 American Chemical Society
Published on Web 09/11/2004

state, this species is a stable hemichrome with no detectable amount of pentacoordinate species at the millimolar concentrations used for NMR experiments. Spectroscopically, S7002 and S6803 Hbs resemble the electron transport protein cytochrome b_5, although, unlike this protein, they are capable of binding exogenous ligands through the release of one of the axial histidines. Perhaps more striking than the ability to form reversible hexacoordinate complexes is S6803 and S7002 Hbs' propensity to attach the heme covalently to the polypeptide via a histidine of the H-helix (His117) and a heme vinyl substituent (*13*, *17*, *18*). As functional information is not yet available for non-nitrogen-fixing cyanobacterial Hbs, the significance and necessity of cross-linking and hexacoordination are open for speculation. Among possible roles, these two features may serve to alter the conformation of the protein, modulate the reactivity of the heme iron, or retain the heme within the globin.

The solution structure of recombinant S6803 Hb prepared by reconstitution of the heme with apoprotein (rHb-R, in which the cross-link is not formed) illustrates the fold adopted by a hexacoordinate trHb. The conformational change that occurs upon replacement of one of the axial ligands with an exogenous ligand cannot be predicted on the basis of this structure alone; however, in the case of S6803 rHb-R, it is expected that the resulting species resembles pentacoordinate relatives such as group I trHb from *Chlamydomonas eugametos* (*5*) with bound cyanide. If so, then the protein structure readjusts significantly upon exogenous ligand binding (*14*).

The goal of the present work was to inspect the changes brought about in the heme cavity by the binding of a diatomic molecule and explore whether H-bonding to the exogenous ligand can be detected in the new conformation. Cyanide was selected because it binds tightly to Fe(III) Hbs (metHbs), exerts a trans effect stabilizing the bond between axial histidine and Fe(III), and conveys convenient low-spin characteristics to the complex. A choice was made to carry out the characterization first of the non-cross-linked form of the protein in order to facilitate comparison with the structure of the hemichrome and its *C. eugametos* relative. Covalent attachment is known to occur spontaneously in the ferric state (*13*), and this uncontrolled reaction poses a problem for physical measurements (*17*), in particular those extending over long periods of time. In studies aimed at probing the properties of site 117 and the mechanism of heme attachment, the reactive histidine was replaced by an alanine in S6803 Hb. H117A S6803 rHb is incapable of covalent heme attachment (*17*, *18*) and, as will be shown here, this protein provided a useful background for further structural studies of the non-cross-linked rHb. By using this variant in the metcyano state, it was possible to determine the fate of the decoordinated axial histidine, identified as His46 (E10), and to observe directly the presence of a hydrogen-bonding network involving the bound cyanide. The influence of the H117A replacement extended to the dynamics of the heme cavity, the rate of cyanide binding, and the distribution of heme orientational isomers. This provided a demonstration of the exquisite control that a single peripheral residue can have on hemoglobin properties.

MATERIALS AND METHODS

Protein Preparation. All reagents were from Sigma (St. Louis, MO) unless otherwise specified. Horse heart myoglobin was obtained from this source and used without further purification. *Synechocystis* sp. PCC 6803 (wild-type and H117A) and *Synechococcus* sp. PCC 7002 hemoglobins were prepared as described previously (*13*, *18*, *19*) by reconstitution of the apoprotein with heme. The genes for H117F S6803 Hb and H117A S7002 Hb were generated by the Stratagene Site Directed Mutagenesis protocol (La Jolla, CA) using oligomers obtained from Integrated DNA Technologies (Coralville, IA). The apo- and holoproteins were expressed in BL21(DE3) cells and purified as reported for the corresponding wild-type proteins (*13*, *19*). Uniformly ^{15}N labeled H117A S6803 rHb was obtained according to established protocols (*16*) using M9 minimal medium enriched with $^{15}NH_4Cl$ (Cambridge Isotopes, Andover, MA). The cyanide complex of the various proteins was prepared by adding an excess of KCN (or $KC^{15}N$, Cambridge Isotopes), adjusting the pH to the value of interest, and incubating at room temperature as necessary. Samples containing imidazole were prepared by addition of aliquots of 0.8 M imidazole (20 mM phosphate, pH 7.2) to 1 mM protein samples (20 mM phosphate buffer, pH 7) followed by incubation. Coarse imidazole titrations were carried out by stepwise addition of imidazole to final concentrations of 10−200 mM.

NMR Spectroscopy. NMR samples were prepared in 20 mM phosphate buffer (95:5 $^1H_2O/^2H_2O$ or "100%" ^2H_2O). Protein concentrations were determined on a per-heme basis using the reported Soret extinction coefficients (*13*, *19*). The concentration was ∼1 mM, except for the collection of natural abundance ^{13}C data (2−4 mM). All NMR spectra were collected at 14.1 T on a Bruker DRX-600 spectrometer. ^1H chemical shifts were referenced to DSS through the water line with correction for pH and temperature (*20*); ^{13}C and ^{15}N were referenced indirectly to the proton frequency (*21*). A summary of the procedures is presented below. Detailed parameters (acquisition and processing) have been reported elsewhere (*13*, *16*, *18*) and are given in the Supporting Information.

Variable-temperature data were collected on H117A S6803 rHbCN (9:1 $^1H_2O/^2H_2O$, 20 mM phosphate) in the range from 7 to 41 °C at pH 7.25. The chemical shift was plotted versus inverse absolute temperature to determine the Curie intercept. Nonselective T_1 values were obtained by inversion recovery with recovery times varying between 1 ms and 3 s. Peak intensities were analyzed with a single-exponential return to equilibrium. The data used in a three-parameter fit (intensity at $t = 0$, at $t = \infty$, and time constant) were limited to recovery times below 1 to 0.5 T_1, for which they adhered to a single-exponential function. The relaxation times were converted into distance to the iron using the relationship (*22*)

$$\frac{T_{1,i}}{T_{1,\mathrm{Me}}} = \frac{R^6_{\mathrm{Fe}-i}}{R^6_{\mathrm{Fe}-\mathrm{Me}}} \quad (1)$$

where i represents the proton of interest, Me a heme methyl

[2] The sequences of trHbs bear little homology to the vertebrate sequences on which the Perutz topological notation was based. Both sequence number and topology are provided where meaningful; in S6803 Hb, the following equivalences hold: Tyr22 (B10), Phe35 (CD1), Gln43 (E7), His46 (E10), Gln47 (E11), Phe50 (E14), and His70 (F8).

Table 1: Selected ^{1}H NMR Chemical Shifts for H117A S6803 rHbCN

	assignment	signal [a]	δ[b]	T_1[c] (ms)	intercept (ppm)
heme	1-methyl	f	12.60	190	7.7
	3-methyl	c	15.06	290	5.2
	5-methyl	d	13.76	237	8.2
	8-methyl		8.28		
	2-α-vinyl	b	15.44		12.5
	trans-2-*β*-vinyl	x	−2.70		6.2
	cis-2-*β*-vinyl	y	−3.99		8.9
	4-α-vinyl		8.59		
	trans-4-*β*-vinyl		1.07		
	cis-4-*β*-vinyl		1.80		
	6-α-propionate	g	12.44		4.6
	6-α′-propionate	h	12.57		4.5
	6-*β*-propionate		1.11		
	6-*β*′-propionate		0.61		
	7-α-propionate	e	13.33	233	
	7-α′-propionate		6.79		
	7-*β*-propionate		0.49		
	7-*β*′-propionate		−0.20		
	α-meso	v	−1.23		20.3
	β-meso		3.72		
	γ-meso		0.74		
	δ-meso		4.21		
His70 (F8)	NH		8.30		
	CαH		6.24		
	C*β*H		6.57		
	C*β*H′		6.36		
	N*δ*H	i	12.18	90	10.6
	C*ϵ*H	z	−7.6		−0.5
	C*δ*H	z′	5.3		
Tyr22 (B10)	O*η*H	a	21.4	52	3.6
	C*ϵ*H	k	8.41		
	C*δ*H		7.32		
Q-2	N*ϵ*2H	w	−1.92	60	12.1

[a] Refer to Figures 8 and S7 for peak labeling and to Figure 3 for the heme nomenclature. [b] In 95:5 $^1H_2O/^2H_2O$, at 35 °C and pH 7.3, from WEFT, WEFT-NOESY, TOCSY, and 1D NOE data. [c] Measured in 95:5 $^1H_2O/^2H_2O$, pH 7.3, 25 °C.

group, and R the distance between the indicated proton(s) and the iron center. The magnitude of heme methyl T_1 values and the trend they exhibit with chemical shift (Table 1) suggest that relaxation processes other than dipolar metal-centered (obeying eq 1) contribute significantly. The heme methyl T_1 value chosen for scaling (240 ms, 5-CH_3, R_{Fe-Me} = 6.1 Å) therefore returns an upper limit of R_{Fe-i}.

One-dimensional steady-state NOE difference spectra were obtained with presaturation of the line of interest (or a signal-free reference frequency) with a 75-ms low-power pulse. One-dimensional WEFT data (*23*) utilized a 200-ms relaxation delay, a 175-ms recovery period, and a 114-ms acquisition. WEFT-NOESY data were collected with 50-ms solvent presaturation, 150-ms inversion recovery time, 20-ms mixing time, and 68-ms acquisition time. The standard complement of 2D data for heme and protein assignment was collected as described elsewhere (*18*); these included NOESY (*24*), WEFT-NOESY (*22*), TOCSY (*25*), and DQF-COSY (*26*) data. Quadrature detection was achieved in the indirect dimension with either the TPPI (*27*) or the States (*28*) method. Water suppression was achieved either with a WATERGATE scheme (*29*) or with presaturation.

Natural abundance $^1H-^{13}C$ HMQC spectra (*30*) were collected at 25 or 35 °C in ^2H_2O with a $1/(2J_{CH})$ 3-ms delay as described elsewhere (*18*). $^1H-^{15}N$ HMQC spectra (*31*) were collected on uniformly ^{15}N-labeled protein with a 15-ms delay. $^1H-^{15}N$ HSQC spectra and ^{15}N-separated NOESY and TOCSY data sets for assignment purposes were collected on uniformly ^{15}N-labeled samples of H117A S6803 rHbCN as described for wild-type S6803 rHb-R (*16*, *32*).

^{15}N spectra were collected at 50.68 MHz on a Bruker AMX2−500 instrument equipped with a 5-mm broad-band probe. Sample temperature was maintained at 17 or 32 °C or was varied up to 37 °C. Data were collected either with a standard pulse−observe sequence (where the pulse was 45° or 90°) or a Hahn−echo sequence (*33*) to eliminate acoustic ringing. A total of 10 000−100 000 transients were accumulated per spectrum with a recycling time of ∼600 ms to allow for the simultaneous detection of the free and bound $C^{15}N^-$ signals.

NMR data were processed using NMRpipe (*34*), XWIN-NMR (Bruker BioSpin, Rheinstetten, Germany), or FELIX (Accelrys, San Diego, CA). The program DmFIT (*35*) was used when spectral simulations were necessary.

Diamagnetic Chemical Shift Calculations. The structure of *Ce* trHbCN [1dly, (*5*)] served as a model to estimate the diamagnetic chemical shifts of residues near the bound cyanide ion. Hydrogen atoms were added to the *Ce* trHbCN structure using XPLOR (*36*), with an adjustment placing the O*η*H atom of Tyr20 (B10) between O*η* and the N atom of the bound cyanide. The observed chemical shift can be expressed as

$$\delta_{obs} = \delta_{dia} + \delta_{con} + \delta_{dip} \quad (2)$$

The first term on the right (δ_{dia}) is the diamagnetic component, which includes primary through tertiary structure effects and ring current effects. The program SHIFTX (*37*) and an in-house ring current shift program were used to calculate δ_{dia} for a few protons of interest in the distal pocket. The paramagnetic contribution ($\delta_{con} + \delta_{dip}$) to protein shifts was not evaluated because of the absence of information on the magnetic susceptibility tensor and experimental diamagnetic shifts.

Heme Electronic Structure. Heme methyl chemical shifts in H117A rHbCN were used to determine the orientation of the axial histidine plane with respect to the plane of the porphyrin macrocycle (*38*). For this calculation, the shifts were corrected for diamagnetic contribution (3.3 ppm). The following heuristic equation was applied:

$$\delta = a \sin^2(\theta - \varphi) + b \cos^2(\theta + \varphi) + c \quad (3)$$

θ represents the angle defined by the Fe−NC vector and the Fe−CH_3 vector, and φ is the angle defined by the Fe−NC vector and the projection of the axial histidine plane onto the porphyrin plane. The lower limits of the reported *a*, *b*, and *c* constants [$a = 18.4 \pm 2.4$, $b = -0.8 \pm 2.0$, $c = 6.1 \pm 1.9$ (*38*)] were used.

Thermal Denaturation. Thermal denaturation experiments were performed as described previously (*16*) using an AVIV Instruments (Lakewood, NJ) model 14D spectrophotometer equipped with a Pelletier device for rapid temperature adjustment. In the case of H117A S6803 hemichrome, a ∼8 *μ*M holoprotein solution (on a per-heme basis) in 20 mM phosphate buffer (pH 7.2) was heated from 25 to 95 °C in 2 °C steps, and spectra were collected between 260 and 700 nm after a 5-min equilibration period. Reversibility was

inspected by refolding the protein from 95 to 26 °C, collecting spectra at 3 °C intervals with 7-min equilibration period. The absorbance at 412 nm was used for data fitting according to a two-state Gibbs−Helmholtz equation adapted for the dependence of the fully folded and fully unfolded signals on temperature (*39*). In the case of H117A S6803 rHbCN, the concentration of protein was ~9 μM on a per heme basis, and the cyanide concentration was set to a 10- or 1000-fold excess. The same heating and cooling protocol was used. The cyanide data were not fit because of obvious deviations from a simple two-state model. In a control experiment, a solution of bis-cyano hemin (with hemin concentration of 8.9 μM and a 1000-fold excess of cyanide) was subjected to the same heating−cooling protocol as the protein.

Kinetics of Cyanide Binding. Cyanide binding was monitored by NMR and absorbance spectroscopy. For samples monitored by NMR spectroscopy, a 2- or 10-fold excess of potassium cyanide was added to a 1 mM sample of H117A rHb and the pH quickly adjusted to 7.3. Successive spectra were obtained as a function of time over several hours. Data obtained by absorbance spectroscopy were collected with protein concentrations of ~10 μM and a 200-, 500-, or 1000-fold excess of cyanide. Spectra were recorded before addition, and the absorbance at 423 nm was monitored throughout the reaction at 30-s intervals up to times allowing for an estimate of the infinity value. A sum of exponential decays was necessary to simulate the concentration data versus time collected under pseudo-first-order conditions. Apparent rate constants were estimated for the major kinetic phase.

RESULTS

Characterization of H117A S6803 rHb in the Hemichrome State. Comparative studies have revealed some of the differences between the non-cross-linked (rHb-R) and cross-linked (rHb-A) forms of the protein in solution (*18*). According to chemical shift information, the structural perturbations are mostly confined to the H-helix and are limited in magnitude. NMR data collected on wild-type rHb-A show that the imidazole ring of the reacted His117 is located in the heme pocket and in dipolar contact obviously with the heme, but also with Phe84. In contrast, the unreacted His117 or rHb-R does not exhibit systematically these proximity relationships, which indicates that the side chain can reorient, perhaps simply with a change in the rotameric state and a minor shift of the H-helix. To prevent the formation of the cross-link [whose existence has been detected in preparations of the soluble holoprotein from *Escherichia coli* (*17*, *19*), but whose role in vivo has not been established], two mutants were considered: H117F S6803 rHb and H117A S6803 rHb. The first was intended as an isosteric mimic and the second to open a cavity near the reactive heme vinyl.

Figure 1 presents the one-dimensional spectra of the wild-type and variant proteins in their hemichrome state. The spectrum of H117F S6803 rHb yielded broad signals and was distinct from the spectrum of wild-type S6803 rHb in the absence of the cross-link. The Phe replacement was therefore found to be unsuitable as a wild-type mimic. In contrast, the spectrum of H117A S6803 rHb resembled

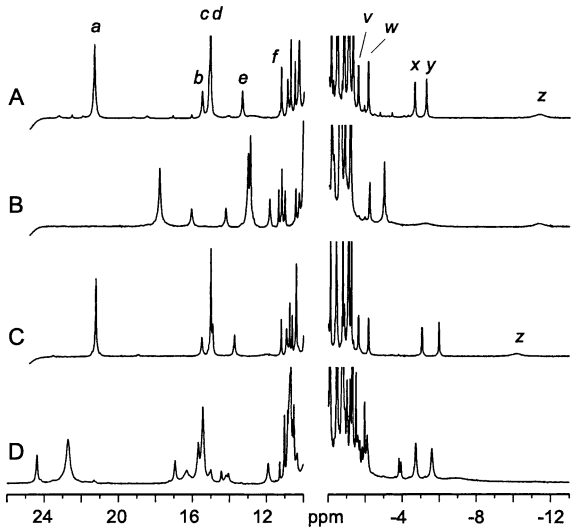

FIGURE 1: ^{1}H NMR spectrum of (A) wild-type S6803 rHb-R, (B) wild-type S6803 rHb-A, (C) H117A S6803 rHb, and (D) H117F S6803 rHb. All samples were in 20 mM phosphate, pH 7.2, 95:5 $^1H_2O/^2H_2O$, and at 25 °C. The chemical shifts of resolved lines in wild-type rHb-R and rHb-A have been reported elsewhere (*16*, *18*). Peak labels are as in ref *16*.

closely that of S6803 rHb-R. A series of homonuclear experiments were performed to examine the geometry of the heme pocket in H117A S6803 rHb. Assignments were obtained for the heme group and a large portion of the protein by comparison of NOE and correlation patterns to those of the wild-type protein. There were few chemical shift deviations between wild-type and H117A S680-3 rHb (Figure S1). The largest differences were observed for the heme 2-vinyl group, for the axial histidines His46 (E10) and His70 (F8), and for the C-terminal portion of the H-helix.

The H-helix of S6803 Hb extends from residue 102 to residue 122 and exhibits a kink near Pro115 (*14*). Sequence analyses reveal a C-cap element before Pro115 and nearly zero helical propensity beyond this residue (*40*−*42*). These propensities are practically unchanged by the H117A replacement. The NMR data supported identical secondary structure in both proteins; however, NOEs unique to the variant placed Ala117 CβH$_3$ in the proximity of the 2-vinyl CβH$_2$ and the ring of Tyr53. This suggested that, on average, the backbone of the H-helix at the level of residue 117 was closer to the heme group than in the wild-type protein and that the replacement of His117 with a small side chain did not open a large cavity near the heme group as originally anticipated.

Aside from contact with Ala117, the environment of the 2-vinyl group consisted of the same residues as in the wild-type protein, with CαH toward the distal side, pointing to Phe50 (E14), and CβH$_2$ toward the proximal side, pointing to Tyr53, Phe84, and Val121 (Figure 2A). The remainder of the heme pocket appeared to be remarkably similar as well. For example, the ring of Phe35 (CD1) exhibited three broad lines at ~6.6, ~7.6, and ~8.6 ppm, as in the wild-type spectrum. The large spread of the shifts, NOEs to the 5-CH$_3$, and line width suggested a location on average close to the heme. Also as in the wild-type protein, the adjacent Phe34 displayed contrastingly sharper lines. Tyr22 (B10) had NOEs to the backbone of Gln43 (E7) (Figure 2B) and Arg44 (E8) as well as the side chain of Leu26. Val121, which is

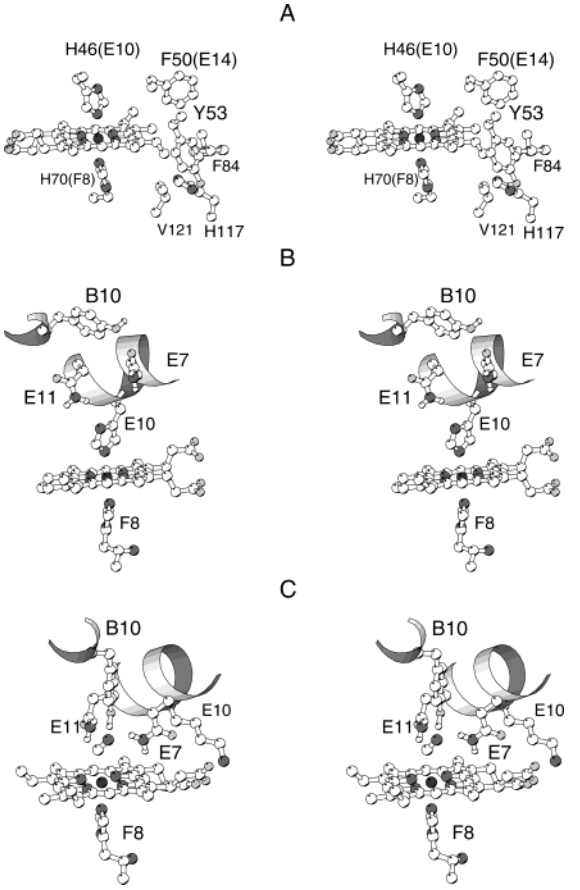

FIGURE 2: (A) Stereoview of the solution structure of wild-type S6803 rHb-R (1mwb, one representative structure, with His117 near the heme group), showing the environment of the heme 2-vinyl and the heme axial ligands His70 (F8) and His46 (E10); the 2-vinyl group should appear front and right. (B) Stereoview of the same structure, showing residues on the distal side of the heme: Tyr22 (B10), Gln43 (E7), and Gln47 (E11). (C) Stereoview of the X-ray structure of *Chlamydomonas eugametos* trHbN (1dly) in the metcyano complex, showing the heme axial ligand His68 (F8) and the distal side of the heme, including Tyr20 (B10), Gln41 (E7), Lys44 (E10), and Gln45 (E11).

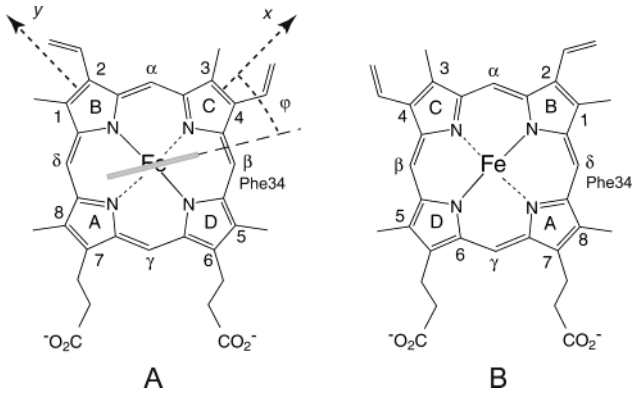

FIGURE 3: Structure of the heme group and the nomenclature used in this work. The projection of the axial histidine imidazole plane is indicated as a gray bar. The orientation of this projection is defined by the angle φ formed with the axis going through the nitrogen atoms of pyrroles A and C. The "major" orientation of the heme group (A) and the "minor" orientation (B) of the heme in the protein are distinguished by a 180° rotation about the $\alpha-\gamma$ meso axis. Phe34 is a fixed protein reference point. In wild-type S803 rHb-R, the ratio of the two isomers is 95:5 at neutral pH and room temperature (*16*).

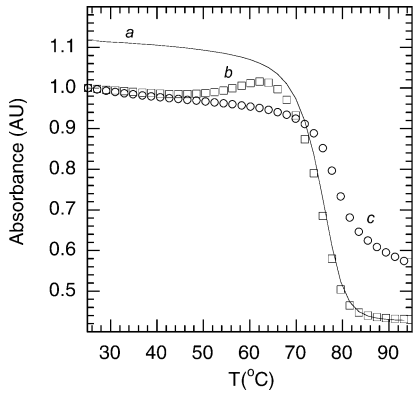

FIGURE 4: Thermal denaturation of H117 S6803 rHb at pH 7.2. The absorbance at 412 nm is followed as a function of temperature. The solid line (a) represents the fit to the hemichrome data. Also shown are the data points for H117 S6803 rHbCN, with a 10-fold excess of KCN (b, □) and a 1000-fold excess of the same (c, ○). The signals were scaled to the same heme concentration in each sample.

one helical turn from position 117, had wild-type interactions with His70 (F8) and the β protons of the heme 2-vinyl group. Furthermore, the proportions of the two isomeric forms, which contained the heme in either of the orientations shown in Figure 3, were unaffected by the replacement. Overall, the H117A substitution appeared to leave the structure of S6803 rHb largely intact.

In an additional control experiment, H117A S6803 rHb was studied for its resistance to thermal denaturation. As the temperature of a buffered solution was increased, the optical spectrum changed from that of a low-spin bis-histidyl compound to that of free, high-spin heme. The set of spectra exhibited nearly perfect isosbestic points at 392 and 589 nm, supporting a two-state process. Figure 4 (trace a) displays the transition observed for absorbance values at 412 nm as a function of temperature. The apparent midpoint for heme loss obtained from two-state fitting of the data was 74.8 °C, within error of the wild-type value [74 °C (*16*)]. Throughout the transition, there was no evidence for the formation of a pentacoordinate species. The optical spectrum of such complex would be expected to resemble that of the Fe(III) H46A mutant reported by Guertin and co-workers (*15*). From the point of view of structure and stability, H117A S6803 rHb was therefore an acceptable candidate for exogenous ligand-binding studies.

Imidazole Binding to Ferric H117A S6803 rHb. To examine the reactivity of the protein, an equivalent amount of imidazole was added to S6803 H117A rHb in the absence of dithionite, and NMR data were recorded on the mixture. A second set of hyperfine-shifted lines became apparent (Figure 5), but the initial spectrum was recovered after gel filtration, which demonstrated that no covalent chemistry had taken place. Increasing the imidazole concentration shifted the equilibrium to the bound form as expected of an equilibrium process. With knowledge of protein and imidazole concentrations, integration of the resolved lines corresponding to free and bound protein forms afforded a dissociation constant of 20 mM. NOESY data collected on a solution approximately at the midpoint of the titration allowed for the assignment of a few of the resonances in slow exchange on the chemical shift time scale (not shown). Shifts in the heme methyl positions revealed a change in

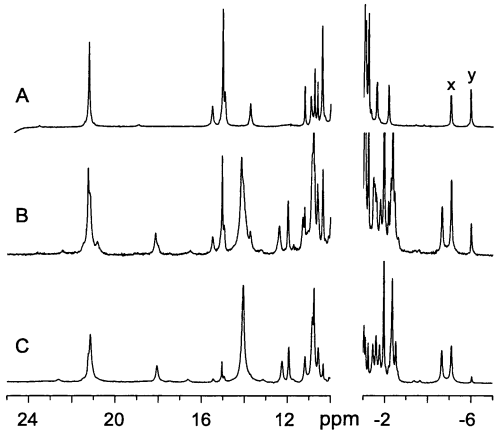

FIGURE 5: Hyperfine-shifted resonances in the ^{1}H NMR spectrum of H117A S6803 rHb (20 mM phosphate, pH 7.2, 95:5 $^1H_2O/^2H_2O$, 25 °C) with (A) 0 mM, (B) 50 mM, and (C) 200 mM imidazole. Peaks labeled x and y correspond to the heme 2-vinyl β protons. In (B) and (C), two sets of such lines are detected. The fraction of imidazole-bound species was determined by spectral simulation.

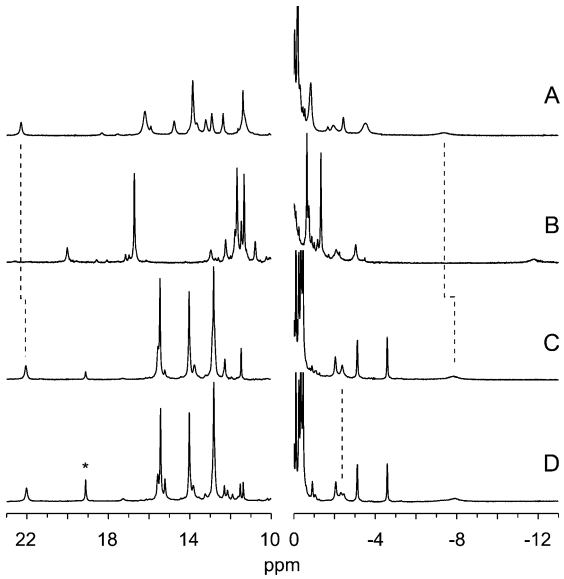

FIGURE 6: Hyperfine-shifted resonances in the ^{1}H NMR spectrum of (A) wild-type S6803 rHb-R, (B) wild type S6803 rHb-A, and (C) H117A S6803 rHb and (D) uniformly ^{15}N-labeled H117A S6803 rHb, all after incubation with a 10-fold excess of KCN. Conditions were 20 mM phosphate, pH 7.2, 95:5 $^1H_2O/^2H_2O$, 25 °C. In spectrum D, $^1J_{NH}$ coupling is clearly visible for an upfield resonance at −2.3 ppm (Q-2 in Table 1). Spectra A, B, and D were scaled using the intensity of the signal at 22 ppm. The * indicates an increase in the minor heme isomer concentration.

electronic structure suggestive of binding directly at the iron ion.

Attempts at a "trans rescue," that is, the formation of a cross-link between heme and imidazole filling in for the His117 ring in H117A S6803 rHb, were made with the dithionite treatment known to work on the wild-type protein. These efforts were unsuccessful even in the presence of a large excess of imidazole (200:1). Remarkably, addition of a 10-fold excess of imidazole to wild-type S6803 rHb-R resulted in low-intensity broad lines that did not parallel the effect on the variant protein. Thus, the H117A replacement in S6803 rHb, although not affecting the structure to a great extent, led to distinct interactions with this ligand. This property was explored further with cyanide, as it generally has a high affinity for Fe(III)PPIX and generates a paramagnetic complex with favorable spectral properties (*22*).

Cyanide Binding by Ferric H117A S6803 rHb. Figure 6 contains the one-dimensional spectra of the metcyano complex of various S6803 rHbs. Although metcyano wild-type S6803 rHb-R exhibited broad lines, the appearance of H117A S6803 rHbCN was comparable to that of wild-type S6803 rHb-R in the hemichrome state (Figure 1). However, the spectra illustrated that cyanide binding was accompanied with an increase in the percentage of minor heme orientational isomer from ∼5% in the hexacoordinate H117A S6803 rHb-R (Figure 1) to >10% in H117A S6803 rHbCN. This was also observed in the related H117A S7002 rHbCN, in which the proportion of minor form reached 30%.

Interestingly, it was necessary to incubate H117A S6803 rHb with cyanide ions for hours to achieve complete conversion of the hemichrome to the metcyano complex. This is shown in Figure 7A, where the intensity of NMR signals from H117A S6803 rHbCN (trace a) and H117A S6803 rHb (trace b) is plotted as a function of time. No intermediate species was detected through the reaction, but extrapolation of the intensity profile back to the time of addition demonstrated the existence of a fast phase accounting for a significant population of the sample. The NMR experiment also revealed a comparatively rapid appearance of the minor isomer (not shown).

Cyanide binding to H117A S6803 rHb was followed optically to access a lower protein concentration regime than possible with NMR spectroscopy. In this experiment, the wavelength of maximum difference between the spectra of H117A S6803 rHb and H117A S6803 rHbCN was used. Three traces are shown in Figure 7B, which were collected at the same protein concentration (11 μM) and with 1000- (trace c), 500- (trace d), and 200-fold (trace e) excesses of cyanide to achieve pseudo-first-order conditions. Unlike the NMR data, which report on the concentration of individual species if the signals are resolved, the absorbance reading has contributions from both heme isomers in both free and bound states at all times. Satisfactory fits of the optical data required multiple exponential terms, as apparent in Figure 7B, which shows a rapid phase and deviation from linearity and longer times. Using the slope of the log plots at the three concentrations, an apparent second-order rate constant of 3.0 $\times$ 10^{-2} M^{-1} s^{-1} was obtained for the major phase. Wild-type data (Figure S2) indicated an apparent rate faster by a factor of ∼8. Pertinent kinetic studies on S6803 rHb in the ferrous state estimate the rate of His46 (E10) decoordination at 930 s^{-1} and a recoordination rate of 4200 s^{-1} (*43*) (pH 7, 20 °C). The apparent second-order rate constant derived above assumes a simple bimolecular mechanism that does not include any such prior or concurrent equilibrium.

Thermal Denaturation of H117A S6803 rHbCN. Thermal denaturation of H117A S6803 rHbCN was performed at low (10-fold excess) and high (1000-fold excess) concentrations of cyanide. Trace b in Figure 4 illustrates the lower concentration transition, and its nonsigmoidal shape provides evidence of departure from two-state behavior. These data could be interpreted with cyanide release and regeneration of the hemichrome at intermediate temperatures. Upon further heating, the absorbance followed the hemichrome

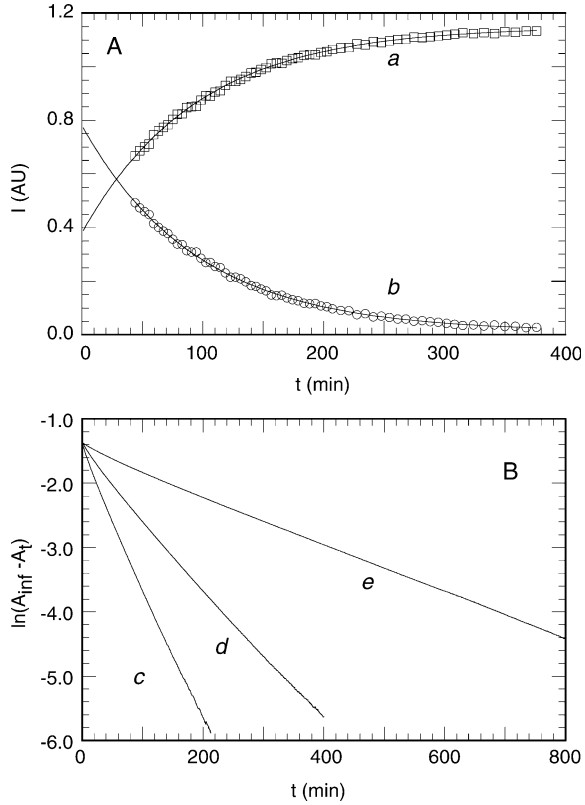

FIGURE 7: Kinetics of cyanide binding to H117A S6803 rHb (pH 7.3, 25 °C). (A) Data for (a) Tyr22 OηH (peak a in Figure 8) and (b) heme 5-CH_3 were obtained by following the intensity of NMR signals (peak d in Figure 8) as a function of time. The protein concentration was 1.1 mM in 9:1 $^1H_2O/^2H_2O$, and KCN was added in a 10-fold excess. The solid lines are shown to guide the eye. The intensities were scaled to approximate the concentration of the sample in mM unit. (B) Absorbance at 423 nm is presented as a log plot under the assumption of pseudo-first-order behavior when a (c) 1000-fold, (d) 500-fold, or (e) 200-fold excess of KCN was added to a 10 μM solution of protein. Deviations from straight lines are apparent at each concentration. By using the middle portion of the curves, pseudo-first-order rate constants of 3.2×10^{-4}, 1.8×10^{-4}, and 6.2×10^{-5} s^{-1} are obtained for curves c, d, and e, respectively.

trace as this species underwent the transition described above (trace a). At high cyanide concentration (Figure 4, trace c), the transition to the hemichrome was abolished, and heme loss occurred through a shallow transition with a midpoint temperature above 75 °C. No clear isosbestic point was obtained in this case. At high temperatures, the spectrum was not identical to that of bis-cyano hemin, although both exhibited a broad shoulder at 610 nm. It is noteworthy that the thermal denaturation of H117A S6803 rHbCN was reversible at this high cyanide concentration, in contrast to the behavior of bis-cyano hemin and the other examined protein solutions. This suggested that the prosthetic group escaped damage and remained nonspecifically associated with the protein matrix at high temperatures.

Heme Resonances in H117A S6803 rHbCN. Heme assignments in H117A S6803 rHbCN were obtained as previously described by combining homonuclear NOE and correlated data (*18*, *22*) and $^1H-^{13}C$ HMQC spectra (Figure S3). The order of the ^1H heme methyl signals was 3−5−1−8, as listed in Table 1. Application of the heuristic equation proposed by Bertini and co-workers (eq 3) to account for heme methyl shifts in His/CN^- complexes (*38*) returned a value of ~ −35° for the projection of the axial imidazole ring on the heme plane with respect to the NA−NC axis, aligning it close to the $\delta-\beta$ meso axis (lying at −45°, Figure 3). This axial histidine orientation is consistent with that of His70 (F8) in wild-type rHb-R (*14*, *18*) and rHb-A (*9*, *18*) and of His F8 in other trHbs (*6*, *44*). Heme assignments were also obtained for H117A S7002 rHbCN. In this case, the methyl order was 5−1−3−8 (Table S1) and the fitted angle was ~ −30°.

Identification of the Axial Histidine in H117A S6803 rHbCN. The signals of the axial histidine were assigned with several homo- and heteronuclear experiments. As a starting point, the $^1H-^{13}C$ HMQC data mentioned above contained a conspicuously shifted CH [$\delta(^{13}C)$ ~66; $\delta(^1H)$ ~6.3] and CH_2 group [$\delta(^{13}C)$ ~23; $\delta(^1H)$ ~6.4 and 6.6]. These shifts were in the range expected of the $\alpha\beta$ moieties of axial histidines (*22*). TOCSY data demonstrated that these were part of the same spin system and connected to a peptide NH at 8.30 ppm. One of the β protons and the NH were in contact with an exchangeable proton at 12.2 ppm, a good candidate for the NδH of the ring because of its 90-ms T_1, placing it 5.2 Å from the iron center (eq 1). The 12.2 ppm proton was connected via one-dimensional steady-state NOEs to the fast relaxing and broad peak at ~ −8 ppm (peak z, Figure 8), assigned as the adjacent CϵH.

Uniformly ^{15}N-labeled protein confirmed the His70 (F8) NH assignment and therefore the rest of the side chain. Three-dimensional data ($^1H-^{15}N$ HSQC-based experiments) provided the ^{15}N shift of the backbone NH (110.3 ppm), and dipolar connectivities typical of helices were identified to Ala69 and Lys71 and their neighbors in the sequence. The data were in agreement with the F-helix pattern of *J* and NOE connectivities reported for the wild-type protein (*14*, *32*) and the H117A hemichrome (this work). $^1H-^{15}N$ HSQC data correlated the 12.2 ppm ^1H signal to a ^{15}N signal at ~148 ppm, a plausible shift for the NδH moiety of an axial histidine (Figure S4). The NδH proton did not experience saturation transfer from the water line at neutral pH. This is normal for axial histidines (*45*, *46*), which are generally not exposed to solvent, and, being committed to iron coordination via their Nϵ atom, experience only base-catalyzed exchange. His70 (F8) NδH is also poised for the formation of a hydrogen bond to the backbone CO of Met66.

Other Histidines in H117A S6803 rHbCN. H117A rHb contains histidines at positions 33, 46 (E10), 70 (F8), 77, and 83. An important aspect of exogenous ligand binding to the heme is the location of His46 (E10) once it is replaced by cyanide. In the TOCSY data of the cyanide complex, four sharp pairs of CδH−CϵH connectivities were observed (not shown), which corresponded to the nonaxial histidines. The line width and shift were characteristic of residues remote (>6 Å) from the paramagnetic center rather than closely associated with the exogenous ligand (*22*). In the cyanide-bound state, His46 (E10) therefore swings out of the heme pocket. Assignment to specific residues could be obtained using the hemichrome information. For example, His83 CϵH had a strong NOE to Asn80 NH (peak j, Figure 8), reflecting the presence of a hydrogen bond involving the Nδ nitrogen and N-capping the G helix. The H-bond stabilizes the NϵH tautomer of the histidine, and His83 displayed a one-bond NϵH connectivity in the $^1H-^{15}N$ HSQC data collected with a WATERGATE solvent suppression (Figure S4). The His83

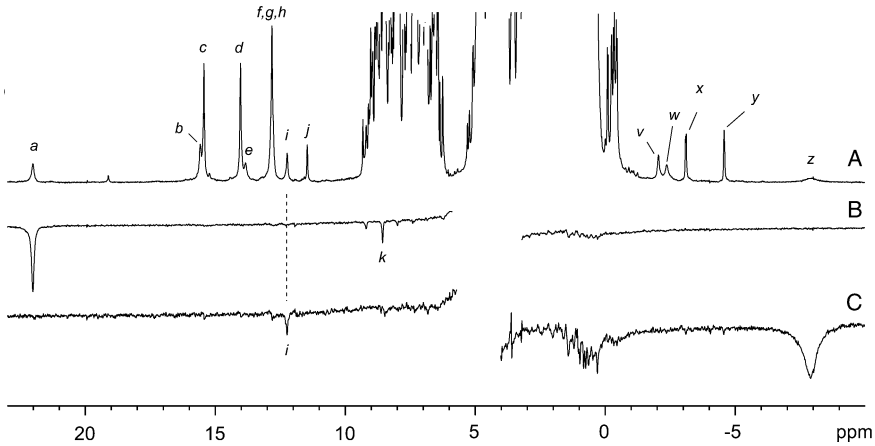

FIGURE 8: Steady-state NOE effects observed in H117A S6803 rHbCN (95:5 $^1H_2O/^2H_2O$, pH 7.3, 25 °C): (A) reference spectrum with peaks labeled as per Table 1; difference spectrum obtained after saturation (75 ms) of (B) peak a and (C) peak z.

NϵH proton, at 11.6 ppm, underwent complete saturation transfer upon irradiation of the water line. Other NOEs matching those in the wild-type or H117A hemichrome were His33 to His83 and Phe34 and His77 to Leu73. The remaining histidine was, by default, His46 (E10).

The $^1H-^{15}N$ HMQC spectrum collected to obtain long-range $^1H-^{15}N$ *J*-coupling information for the imidazole rings (*31*) returned patterns typical of the NϵH tautomeric state for His33 and His83 (Figure S5). At neutral pH, the signals from His77 and His46 (E10) were not detected, likely because of exchange between the protonated and unprotonated states on a time scale resulting in broadening of the ^{15}N signals. Broad ^{15}N signals were indeed observed in the ^{15}N spectrum of the labeled protein (Figure S6). The similarity of the HMQC data to those collected on wild-type S6803 rHb-R (*18*) suggested His83, His33, and His77 had unchanged pK_a values.

Heme Pocket Residues in H117A S6803 rHbCN. The *Ce* HbCN model predicted that further structural changes should be observed upon cyanide binding. In this protein (Figure 2), Tyr20 (B10) points directly to the bound cyanide, with Oη within 5.5 Å of the iron ion and within 2.4 Å of the cyanide nitrogen. The cyanide N atom is 2.9 Å from *Ce* Gln41 (E7) Nϵ2 and forms a second H-bond to it. Also part of this network is Gln45 (E11), with Nϵ2 within 3.0 Å of Tyr20 (B10) Oη. In H117A S6803 rHbCN, these three residues (Tyr22, Gln43, and Gln47) were also expected in the direct environment of the bound cyanide, and under the influence of the paramagnetic center.

The assignments described above accounted for all downfield hyperfine shifted signals observed in ^1H_2O, except an exchangeable peak at 22 ppm (peak a, Figure 8). This proton did not experience saturation transfer from the bulk water, had a large temperature coefficient (shift at infinite temperature, or Curie intercept, of 3.6 ppm; Table 1), and a T_1 value of 52 ms, shorter than observed for the NδH of His70 (F8). These parameters placed the 22 ppm proton at ~4.7 Å to the Fe(III) ion and in a position such that the dipolar contribution to the hyperfine shift was large. The 22 ppm signal remained a singlet in the ^{15}N-labeled protein spectrum (Figure 6) and exhibited a strong NOE to a signal (8.53 ppm, peak k in Figure 8) belonging to an AX system and *J*-correlated to a ^{13}C signal (117 ppm) in the tyrosine Cϵ region (Figure S3). Each of these observations was in agreement with the 22 ppm signal originating from Tyr22 (B10) OηH involved in a hydrogen bond. NOEs between the ring of Tyr22 (B10) and a phenylalanine ring (Phe21) were consistent with the *Ce* trHbCN geometry. Only one signal was detected per pair of CδH's and CϵH's, which implied that the ring of Tyr22 (B10) was freely rotating on the chemical shift time scale. This is unlike Tyr B10 in *Ascaris suum* HbCN, where rotational averaging was imperfect and contributed to the broad line width of the ring protons (*47*).

The $^1H-^{15}N$ HSQC data collected on uniformly ^{15}N-labeled H117A S6803 rHbCN contained two NH_2 groups with shifts out of the ordinary (Figure S4). The first pair (Q-1) resonated at 99 (^{15}N), 9.17, and 4.14 ppm, the former proton exhibiting a strong NOE to Tyr22 (B10) OηH. The second pair (Q-2) occurred at 103 (^{15}N), 6.27, and −2.35 ppm, the latter proton relaxing with a nonselective T_1 of ~60 ms, corresponding to a 4.8-Å distance to the iron (eq 1). Weak NOEs between both protons of this NH_2 and Tyr22 (B10) OηH confirmed the distal location of the side chain. According to the structure of *Ce* trHbCN, the amide proton closest to Tyr22 (B10) OηH belonged to Gln43 (E7) and matched the first NH_2 pair, Q-1. The second NH_2 pair, Q-2, would arise from Gln47 (E11).

The side-chain amide protons of Gln41 (E7) and Gln45 (E11) in *Ce* trHbCN, by virtue of their location with respect to the porphyrin macrocycle, are expected to experience large upfield ring-current shifts (estimated to range from −2 to −3.2 ppm). Combining these values with those calculated with SHIFTX returned diamagnetic shifts between 3.5 and 5.5 ppm. This suggested that the same four protons in H117A S6803 HbCN exhibited positive and negative dipolar contributions to the paramagnetic shift, a feature that will be useful when the orientation of the magnetic susceptibility tensor is determined. The geometrical parameters of interest are the plane of the proximal imidazole and the tilt of the axial ligands (*47*, *48*). The imidazole plane in *Ce* trHbCN and S6803 rHbCN (see above) is nearly aligned with the $\delta-\beta$ axis; the tilt of the bound CN^- ion, which is large in the *Ce* trHbCN structure (~51°), is not known in H117A S6803 rHb, but with additional information could be determined on the basis of paramagnetic shifts (*47*). In H117A S6803 rHb, this is rendered difficult by the absence

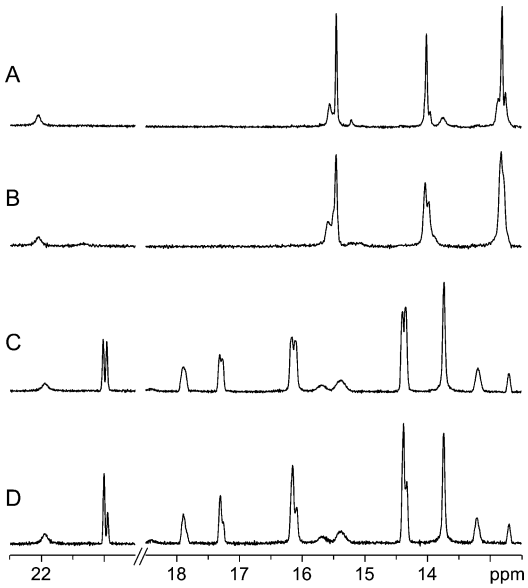

FIGURE 9: Downfield hyperfine-shifted portion of the ^{1}H NMR spectrum of H117A S6803 rHb-CN in (A) 95:5 $^1H_2O/^2H_2O$ and (B) 1:1 $^1H_2O/^2H_2O$ and of H117A S7002 rHb-CN in (C) 1:1 $^1H_2O/^2H_2O$ and (D) in 7:3 $^1H_2O/^2H_2O$. Other conditions were 20 mM phosphate, pH 7.3, 25 °C, and 10-fold excess of cyanide. Heme methyl assignments are listed in Tables 1 and S1.

of suitable diamagnetic reference and will be considered elsewhere.

Several other residues were assigned in the heme pocket. On the proximal side, the same network of dipolar contacts as in the hemichrome state is observed: His83 to Leu79; Leu79 to 4-vinyl; Leu73 to 5-CH_3, Leu79, and His77; Phe34 to 4-vinyl; Phe50 (E14) to 1-CH_3 and 8-CH_3; Val121 to Phe84 and His70 (F8); Ala117 to 2-vinyl. Among the side chains affected by cyanide binding was Phe50 (E14), which in the hemichrome had NOEs to the 2-vinyl group but in HbCN shifted toward the heme δ meso position. Ala117 also appeared to be farther from the 2-vinyl. The lines from Phe34 remained sharp and those from Phe35 (CD1), broad. Phe35 (CD1) was in contact with Tyr22 (B10), and, along with Phe21 (B9) and Val25 (B13), defined a hydrophobic niche for this residue.

Hydrogen-Bonding Network in H117A rHbCN. In favorable circumstances, hydrogen bonds to the heme ligand can be identified through ^{1}H/^{2}H isotope effects (*49*). When spectra of H117A S6803 rHbCN were recorded in mixtures of ^1H_2O and ^2H_2O, two resolved heme methyl signals were found to split into two components, weighted in proportion of the isotopic composition of the solvent. This was particularly obvious in H117A S7002 HbCN and is illustrated in Figure 9. In this spectrum, the lines from the resolved 5-, 1-, and 3-CH_3 (major isomer) and 3-CH_3 (minor isomer) are clearly doubled. The two transitions could be attributed to distinct electronic structures of the heme caused by hydrogen bonding to either ^{1}H or ^{2}H. As observed in sperm whale metMbCN, the downfield component was associated with the presence of ^{1}H and the upfield component with that of ^{2}H. Also as in metMbCN, the chemical shift difference between the two lines ($\sim$30 Hz) indicated a time scale for the ^{1}H/^{2}H exchange process slower than 10^{-2} s^{-1}. The isotope splitting confirmed hydrogen bonding to the ligand, but it is noteworthy that only two sets of lines were observed, each corresponding to the pure isotope shifts.

^{15}N Chemical Shift of Bound Cyanide. ^{15}N spectra were recorded with ^{15}N-labeled cyanide to gain further insight into the electronic structure of the complex (*50*). Horse myoglobin was used as a control sample. In our hands, $C^{15}N^-$ bound to horse metMb resonated at 1352 ppm (in 95:5 $^1H_2O/^2H_2O$, pH 8.3, 17 °C, with respect to liquid NH_3). The difference in shift between bound and free ^{15}N-labeled cyanide was 1102 ppm (see Table S2 for additional values). In contrast, the downfield shifts observed for the cyanide bound to cyanobacterial globins were not as pronounced. H117A S6803 rHbC^{15}N displayed a value of 939 ppm (in 95:5 $^1H_2O/^2H_2O$, pH 7.3, 32 °C) and H117A S7002 rHbC^{15}N a value of 951 ppm (in ^1H_2O, pH 8.4, 17 °C; 698 ppm from free cyanide). Variable-temperature data were collected on H117A S7002 rHbC^{15}N; over the narrow range of temperatures that was tested, the signal shifted upfield linearly with 1/*T*. The intercept at infinite temperature was 332 ppm, lower than the value reported for the parent diamagnetic compound [263 ppm (*51*)]; the limited range of temperature and undetected deviations from linearity could readily explain the discrepancy. The bound $C^{15}N^-$ chemical shifts are to be compared with the values reported by others for hemoglobins, myoglobins, and cytochrome *c* (*50*, *52*) and also with peroxidases (*51*). Among these, H117A S6803 and S7002 rHbCN compare best with horseradish peroxidase.

DISCUSSION

Replacement of His117 by an alanine or a phenylalanine elicited different NMR spectral responses in S6803 rHb. The bulky Phe117 changed the proportions of heme orientational isomers, shifting and broadening several hyperfine signals. These manifestations were not observed in the His117Ala variant, but in this protein, the H-helix moved toward the heme group at the level of the new alanine. The residue occupying position 117 therefore influenced the structure and dynamics of the heme pocket. This was confirmed with differences in the way the wild-type and mutant proteins bound small exogenous ligands such as imidazole and cyanide. That a single amino acid is capable of affecting multiple holoprotein properties has been documented extensively in hemoglobins (*11*) and cytochrome b_5, a bis-histidyl *b* hemoprotein (see, for example, refs *53* and *54*). Position 117 appeared to be a sensitive location in S6803 rHb even though it is at the edge of the heme cavity on the proximal side.

The NMR spectra collected on the metcyano complex of H117A S6803 rHb provided evidence for the replacement of the distal-side histidine by the exogenous ligand. This behavior was consistent with that of other hexacoordinate hemoglobins (*3*, *55*) and published data on His46 (E10) mutants of S6803 rHb (*15*). Furthermore, the reorientation of His46 (B10) outside the influence of the paramagnetic center was in agreement with structural features of *Ce* trHbCN, which has Lys44 (E10) pointing to the solvent (*5*). The reason for the disparity in the behavior of His70 (kinetically stable) and His46 (replaceable) in S6803 rHb is not clear and is in contrast with hexacoordinate systems such as cytochrome b_5, which does not bind cyanide ions. X-ray data on S6803 rHb-A, unlike NMR data (*14*), can provide precise information on the geometry of the axial histidines and support a difference due to increased bond length and

tilt angle (*9*). It is possible that the conformation attained when His46 (E10) is displaced by an exogenous ligand is comparatively strain-free and energetically favored.

A recent study of the kinetics of cyanide association with pentacoordinate trHbs reports $k_{on} = 4.6 \times 10^2$ M^{-1} s^{-1} at pH 7.0 and 20 °C for *Ce* trHbN (*56*). Binding was found to be slower by decades in H117A S6803 rHb. The kinetics of the reaction involving mammalian metMb (His/H_2O axial ligands) have been extensively studied by Ikeda-Saito and co-workers, who identified the major factors controlling the association rate: acid dissociation constant of HCN in the heme pocket, steric hindrance and electrostatic interactions at the distal site, and strength of water coordination (*57*). For hexacoordinate hemoglobins such as S6803 rHb, the latter effect is replaced by the kinetic lability of the distal histidine; a large-scale conformational change coupled to binding may also play a role. Cyanide binding as slow as reported here is rare (*58*); in the hexacoordinate neuroglobin (*59*), it was linked to the rupture of the Fe−His(E7) bond. This was not the case for (H117A) S6803 rHb because a first-order dependence on cyanide concentration was observed at high cyanide concentrations. As mentioned under Results, the rate constants for ligation and deligation of His46 (E10) are fast compared to the observed rate. Assuming these constants are not affected to an extreme extent by oxidation to Fe(III) and the H117A replacement (and possibly the cross-link in the wild-type protein), they also support a rate-limiting step distinct from decoordination. The barrier could arise from a cyanide-dependent heme pocket rearrangement leading to the final state, which contains displaced and rotated E and B helices. This rearrangement would be conditioned by the nature of the residue at position 117, perhaps through a repositioning of the heme group in its site. Alternative interpretations for the slower rate exhibited by H117A S6803 rHb call for a decrease in the efficiency of HCN dissociation caused by a modified electrostatic environment, as for other Hbs (*56*−*58*), and possibly hindered access to the heme pocket. The structural and dynamic properties of the H117F and H117A variants and a recent study of cavities in trHbN identifying a Xe-binding site near the 2-vinyl group (site 2) (*8*) lend support to this view. The observation that the minor heme orientational isomer, which has the 3-CH_3 in place of the 2-vinyl, reacts more quickly than the major isomer also suggests that the conformation near position 117 is critical. Finally, heme reorientation is likely to involve large-scale motions of the heme pocket, altering channels and cavities. In S6803 rHb-R, it is only marginally slower (*16*) than the rate of cyanide binding under large excess conditions.

The NMR data, although partial, were useful to describe structural details of the S6803 rHb pocket in solution. For example, His70 (F8) adopted an orientation comparable to that in certain heme oxygenases (*60*, *61*) and presumed to strengthen the Fe(II)−His bond by relieving steric strain with the pyrrole nitrogens (*62*). Also distinct from typical hologlobin properties was the ^{15}N shift of the bound cyanide; the closest match was with some peroxidases (*51*), the reduced shifts of which have been attributed to H-bonding, the imidazolate character of the histidine in trans, and the tilt of the cyanide ion from the heme normal, all factors that are thought to modulate function. The observed CϵH shift and average CβH shift of His70 (F8) are small (Table 1) compared to those in peroxidases, suggesting a small contact contribution and therefore that the imidazolate character of His70 (F8) is not particularly high (*63*).

In another unusual manifestation, the ratio of heme orientational isomers was seen to depend on the bound ligand, with cyanide decreasing the ability of the protein matrix to discriminate between the two states. A similar observation has been reported for neuroglobin (*59*). For vertebrate globins, it is generally assumed that the rate of association of heme and apoprotein to form the holoprotein is independent of the protein (*64*) and heme orientation (*65*). This implies that the affinity for the heme group, and therefore the equilibrium ratio of isomer concentrations, is dictated by the rate of heme release from the protein matrix. Vertebrate globins tend to experience a relatively modest conformational change upon small exogenous ligand binding. The structural rearrangement following cyanide binding in S6803 rHb is significant, leading to the repositioning of Phe50 (E14) and other pocket residues; these altered interactions may well dictate a different rate of heme loss and therefore a different equilibrium ratio. In addition, there are intrinsic distal differences between the hemichrome and the metcyano complex. Thus, the ligation of His46 (E10) may impose steric constraints that are partially relaxed when the ligating moiety is converted into a cyanide ion forming a H-bond with Tyr22 (B10).

The large structural changes triggered by the binding of cyanide result in a stable H-bonding network as reported for other trHbs. However, solutions of H117A S6803 rHbCN in mixtures of ^1H_2O and ^2H_2O established the predominance of one hydrogen bond to the cyanide ligand, likely with Tyr22 (B10) OηH as the donor because of the unusually slow exchange exhibited by this hydroxyl proton and its chemical shift strongly affected by the paramagnetic center. The distance between the H-bonded phenolic OH and the Fe atom in *Ce* trHbCN was calculated to be 4.4 Å on the basis of the X-ray structure, shorter than that obtained by T_1 measurements in H117A S6803 rHbCN (∼4.7 Å). This could be due to an overestimation of the distance but could also reflect that the tilt of the cyanide is not as pronounced in the latter protein. Evidence was found for a close interaction between Tyr22 (B10) and the amide group of a glutamine, tentatively Gln43 (E7); Tyr22 (B10) is also near a second amide group, from Gln47 (E11).

The role of H-bonding networks involving the ligand, Tyr B10, Gln E7, and Gln E11, in tuning the oxygen affinity has been extensively studied in invertebrate globins (*10*, *11*). It is now possible to anticipate some of the properties conveyed by protein composition near the exogenous ligand, as illustrated by the minihemoglobin from *Cerebratulus lacteus* (containing Thr E11, low O_2 affinity) and the hemoglobin from *Ascaris suum* (containing Ile E11, high O_2 affinity) (*66*). A recent study of NO-bound *Mycobacterium tuberculosis* trHbN, a protein that contains Tyr B10 and Gln E11, establishes a role for Tyr B10 in positioning the exogenous ligand (*4*) through H-bonding interactions. Interestingly, the NO binding appears to have long-range structural effects extending to the loop leading into the F helix. A similar effect may be propagated from site 117 in the cyanobacterial Hb to the CN^-−B10−E7−E11 network.

Even though the His117Ala mutation in S6803 rHb caused slight changes in the resting hexacoordinate state, it exerted a remarkable influence on ligand binding. An extension of

this observation proposes that the cross-link of rHb-A also modifies the properties of the protein, a hypothesis that is currently being tested. Furthermore, bis-histidyl hexacoordination appeared to have little impact with respect to heme reorientation, protein stability, and cyanide binding. In this case, ligand switching from exogenous to endogenous may serve a structural role, providing a mechanism for a large conformational change.

ACKNOWLEDGMENT

We thank Dr. Dan Jones for mass spectrometry analyses, Nancy Scott for assistance in the preparation of plasmids and proteins, and Kunal Mukhopadhyay for assistance with optical data collection. Figure 2 was prepared with MOLSCRIPT (*67*).

SUPPORTING INFORMATION AVAILABLE

Seven figures and two tables: Figure S1, ^{1}H chemical shift differences between S6803 rHb-R and H117A S6803 rHb; Figure S2, kinetics of cyanide binding to wild-type and H117A S6803 rHb; Figure S3, $^{1}H-^{13}C$ HMQC spectrum of H117A S6803 rHbCN; Figure S4, $^{1}H-^{15}N$ HSQC spectrum of H117A S6803 rHbCN; Figure S5, $^{1}H-^{15}N$ HMQC spectrum of H117A S6803 rHbCN; Figure S6, ^{15}N spectrum of H117A S6803 rHbC^{15}N; Figure S7, WEFT spectrum of H117A S6803 rHbCN; Table S1, selected ^{1}H chemical shifts for H117A S7002 rHbCN; Table S2, ^{15}N chemical shift for bound cyanide in selected proteins. This material is available free of charge via the Internet at http://pubs.acs.org.

REFERENCES

1. Wittenberg, J. B., Bolognesi, M., Wittenberg, B. A., and Guertin, M. (2002) Truncated hemoglobins: A new family of hemoglobins widely distributed in bacteria, unicellular eukaryotes and plants, *J. Biol. Chem. 277*, 871−874.
2. Ouellet, H., Ouellet, Y., Richard, C., Labarre, M., Wittenberg, B., Wittenberg, J., and Guertin, M. (2002) Truncated hemoglobin HbN protects *Mycobacterium bovis* from nitric oxide, *Proc. Natl. Acad. Sci. U.S.A. 99*, 5902−5907.
3. Couture, M., Das, T. K., Lee, H. C., Peisach, J., Rousseau, D. L., Wittenberg, B. A., Wittenberg, J. B., and Guertin, M. (1999) *Chlamydomonas* chloroplast ferrous hemoglobin. Heme pocket structure and reactions with ligands, *J. Biol. Chem. 274*, 6898−6910.
4. Mukai, M., Ouellet, Y., Ouellet, H., Guertin, M., and Yeh, S. R. (2004) NO binding induced conformational changes in a truncated hemoglobin from *Mycobacterium tuberculosis*, *Biochemistry 43*, 2764−2770.
5. Pesce, A., Couture, M., Dewilde, S., Guertin, M., Yamauchi, K., Ascenzi, P., Moens, L., and Bolognesi, M. (2000) A novel two-over-two α-helical sandwich fold is characteristic of the truncated hemoglobin family, *EMBO J. 19*, 2424−2434.
6. Milani, M., Pesce, A., Ouellet, Y., Ascenzi, P., Guertin, M., and Bolognesi, M. (2001) *Mycobacterium tuberculosis* hemoglobin N displays a protein tunnel suited for O_2 diffusion to the heme, *EMBO J. 20*, 3902−3909.
7. Samuni, U., Dantsker, D., Ray, A., Wittenberg, J. B., Wittenberg, B. A., Dewilde, S., Moens, L., Ouellet, Y., Guertin, M., and Friedman, J. M. (2003) Kinetic modulation in carbonmonoxy derivatives of truncated hemoglobins: the role of distal heme pocket residues and extended apolar tunnel, *J. Biol. Chem. 278*, 27241−27250.
8. Milani, M., Pesce, A., Ouellet, Y., Dewilde, S., Friedman, J., Ascenzi, P., Guertin, M., and Bolognesi, M. (2004) Heme-ligand tunneling in group I truncated hemoglobins, *J. Biol. Chem. 279*, 21520−21525.
9. Hoy, J. A., Kundu, S., Trent, J. T., 3rd, Ramaswamy, S., and Hargrove, M. S. (2004) The crystal structure of *Synechocystis* hemoglobin with a covalent heme linkage, *J. Biol. Chem. 279*, 16535−16542.
10. Bolognesi, M., Bordo, D., Rizzi, M., Tarricone, C., and Ascenzi, P. (1997) Nonvertebrate hemoglobins: structural bases for reactivity, *Prog. Biophys. Mol. Biol. 68*, 29−68.
11. Weber, R. E., and Vinogradov, S. N. (2001) Nonvertebrate hemoglobins: functions and molecular adaptations, *Physiol. Rev. 81*, 569−628.
12. Kaneko, T., Sato, S., Kotani, H., Tanaka, A., Asamizu, E., Nakamura, Y., Miyajima, N., Hirosawa, M., Sugiura, M., Sasamoto, S., Kimura, T., Hosouchi, T., Matsuno, A., Muraki, A., Nakazaki, N., Naruo, K., Okumura, S., Shimpo, S., Takeuchi, C., Wada, T., Watanabe, A., Yamada, M., Yasuda, M., and Tabata, S. (1996) Sequence analysis of the genome of the unicellular cyanobacterium *Synechocystis* sp. strain PCC6803. II. Sequence determination of the entire genome and assignment of potential protein-coding regions, *DNA Res. 3*, 109−136.
13. Scott, N. L., Falzone, C. J., Vuletich, D. A., Zhao, J., Bryant, D. A., and Lecomte, J. T. J. (2002) The hemoglobin of the cyanobacterium *Synechococcus* sp. PCC 7002: evidence for hexacoordination and covalent adduct formation in the ferric recombinant protein, *Biochemistry 41*, 6902−6910.
14. Falzone, C. J., Vu, B. C., Scott, N. L., and Lecomte, J. T. J. (2002) The solution structure of the recombinant hemoglobin from the cyanobacterium *Synechocystis* sp. PCC 6803 in its hemichrome state, *J. Mol. Biol. 324*, 1015−1029.
15. Couture, M., Das, T. K., Savard, P. Y., Ouellet, Y., Wittenberg, J. B., Wittenberg, B. A., Rousseau, D. L., and Guertin, M. (2000) Structural investigations of the hemoglobin of the cyanobacterium *Synechocystis* PCC 6803 reveal a unique distal heme pocket, *Eur. J. Biochem. 267*, 4770−4780.
16. Lecomte, J. T. J., Scott, N. L., Vu, B. C., and Falzone, C. J. (2001) Binding of ferric heme by the recombinant globin from the cyanobacterium *Synechocystis* sp. PCC 6803, *Biochemistry 40*, 6541−6552.
17. Vu, B. C., Jones, A. D., and Lecomte, J. T. J. (2002) Novel histidine-heme covalent linkage in a hemoglobin, *J. Am. Chem. Soc. 124*, 8544−8545.
18. Vu, B. C., Vuletich, D. A., Kuriakose, S. A., Falzone, C. J., and Lecomte, J. T. (2004) Characterization of the heme-histidine cross-link in cyanobacterial hemoglobins from *Synechocystis* sp. PCC 6803 and *Synechococcus* sp. PCC 7002, *J. Biol. Inorg. Chem. 9*, 183−194.
19. Scott, N. L., and Lecomte, J. T. J. (2000) Cloning, expression, purification, and preliminary characterization of a putative hemoglobin from the cyanobacterium *Synechocystis* sp. PCC 6803, *Protein Sci. 9*, 587−597.
20. Wishart, D. S., Bigam, C. G., Yao, J., Abildgaard, F., Dyson, H. J., Oldfield, E., Markley, J. L., and Sykes, B. D. (1995) ^{1}H, ^{13}C and ^{15}N chemical shift referencing in biomolecular NMR, *J. Biomol. NMR 6*, 135−140.
21. Live, D. H., Davis, D. G., Agosta, W. C., and Cowburn, D. (1984) Long-range hydrogen bond mediated effects in peptides: ^{15}N NMR study of gramicidin S in water and organic solvents, *J. Am. Chem. Soc. 106*, 1939−1941.
22. La Mar, G. N., Satterlee, J. D., and de Ropp, J. S. (1999) in *The Porphyrin Handbook* (Smith, K. M., Kadish, K., and Guilard, R., Eds.) pp 185−298, Academic Press, Burlington, MA.
23. Inubushi, T., and Becker, E. D. (1983) Efficient detection of paramagnetically shifted NMR resonances by optimizing the WEFT pulse sequence, *J. Magn. Reson. 51*, 128−133.
24. Kumar, A., Ernst, R. R., and Wüthrich, K. (1980) A 2D NOE experiment for the elucidation of complete proton−proton cross-relaxation networks in biological macromolecules, *Biochem. Biophys. Res. Commun. 95*, 1−6.
25. Cavanagh, J., and Rance, M. (1992) Suppression of cross-relaxation effects in TOCSY spectra via a modified DIPSI-2 mixing sequence, *J. Magn. Reson. 96*, 670−678.
26. Rance, M., Sørensen, O. W., Bodenhausen, G., Wagner, G., Ernst, R. R., and Wüthrich, K. (1983) Improved spectral resolution in COSY ^{1}H NMR spectra of proteins via double quantum filtering, *Biochem. Biophys. Res. Commun. 117*, 479−485.
27. Marion, D., and Wüthrich, K. (1983). Application of phase sensitive two-dimensional correlated spectroscopy (COSY) for measurements of $^{1}H-^{1}H$ spin−spin coupling constants in proteins, *Biochem. Biophys. Res. Commun. 113*, 967−974.
28. States, D. J., Haberkorn, R. A., and Ruben, D. J. (1982) A two-dimensional nuclear Overhauser experiment with pure absorption phase in four quadrants, *J. Magn. Reson. 48*, 286−292.

29. Piotto, M., Saudek, V., and Sklenár, V. (1992) Gradient-tailored excitation for single-quantum NMR spectroscopy of aqueous solutions, *J. Biomol. NMR 2*, 661−665.
30. Mueller, L. (1979) Sensitivity enhanced detection of weak nuclei using heteronuclear multiple quantum coherence, *J. Am. Chem. Soc. 101*, 4481−4484.
31. Pelton, J. G., Torchia, D. A., Meadow, N. D., and Roseman, S. (1993) Tautomeric states of the active-site histidines of phosphorylated and unphosphorylated IIIGlc, a signal-transducing protein from *Escherichia coli*, using two-dimensional heteronuclear NMR techniques, *Protein Sci. 2*, 543−558.
32. Falzone, C. J., and Lecomte, J. T. J. (2002) Letter to the Editor: Assignment of the ^{1}H, ^{13}C, and ^{15}N signals of *Synechocystis* sp. PCC 6803 methemoglobin, *J. Biomol. NMR 23*, 71−72.
33. Rance, M., and Byrd, R. A. (1983) Obtaining high-fidelity spin-1/2 powder spectra in anisotropic media: phase-cycled Hahn echo spectroscopy, *J. Magn. Reson. 52*, 221−240.
34. Delaglio, F., Grzesiek, S., Vuister, G. W., Zhu, G., Pfeifer, J., and Bax, A. (1995) NMRPipe: a multidimensional spectral processing system based on UNIX pipes, *J. Biomol. NMR 6*, 277−293.
35. Massiot, D., Fayon, F., Capron, M., King, I., Le Calve, S., Alonso, B., Durand, J. O., Bujoli, B., Gan, Z. H., and Hoatson, G. (2002) Modelling one- and two-dimensional solid-state NMR spectra, *Magn. Reson. Chem. 40*, 70−76.
36. Brünger, A. T. (1992) *X-PLOR. Version 3.1. A System for X-ray Crystallography and NMR*, Yale University Press, New Haven, CT.
37. Neal, S., Nip, A. M., Zhang, H., and Wishart, D. S. (2003) Rapid and accurate calculation of protein ^{1}H, ^{13}C and ^{15}N chemical shifts, *J. Biomol. NMR. 26*, 215−240.
38. Bertini, I., Luchinat, C., Parigi, G., and Walker, F. A. (1999) Heme methyl ^{1}H chemical shifts as structural parameters in some low-spin ferriheme proteins, *J. Biol. Inorg. Chem. 4*, 515−519.
39. Pace, C. N., Shirley, B. A., and Thomson, J. A. (1989) *Protein Structure: A Practical Approach*, IRL Press, Oxford, U.K.
40. Muñoz, V., and Serrano, L. (1995) Elucidating the folding problem of helical peptides using empirical parameters. II. Helix macrodipole effects and rational modification of the helical content of natural peptides, *J. Mol. Biol. 245*, 275−296.
41. Muñoz, V., and Serrano, L. (1995) Elucidating the folding problem of helical peptides using empirical parameters. III. Temperature and pH dependence, *J. Mol. Biol. 245*, 297−308.
42. Aurora, R., and Rose, G. D. (1998) Helix capping, *Protein Sci. 7*, 21−38.
43. Hvitved, A. N., Trent, J. T., 3rd, Premer, S. A., and Hargrove, M. S. (2001) Ligand binding and hexacoordination in *Synechocystis* hemoglobin, *J. Biol. Chem. 276*, 34714−34721.
44. Milani, M., Savard, P. Y., Ouellet, H., Ascenzi, P., Guertin, M., and Bolognesi, M. (2003) A TyrCD1/TrpG8 hydrogen bond network and a TyrB10-TyrCD1 covalent link shape the heme distal site of *Mycobacterium tuberculosis* hemoglobin O, *Proc. Natl. Acad. Sci. U.S.A. 100*, 5766−5771.
45. La Mar, G. N., Cutnell, J. D., and Kong, S. B. (1981) Proton magnetic resonance characterization of the dynamic stability of the heme pocket in myoglobin by the exchange behavior of the labile proton of the proximal histidyl imidazole, *Biophys. J. 34*, 217−226.
46. Lecomte, J. T. J., and La Mar, G. N. (1985) ^{1}H NMR study of labile proton exchange in the heme cavity as a probe for the potential ligand entry channel in myoglobin, *Biochemistry 24*, 7388−7395.
47. Xia, Z., Zhang, W., Nguyen, B. D., Mar, G. N., Kloek, A. P., and Goldberg, D. E. (1999) ^{1}H NMR investigation of the distal hydrogen bonding network and ligand tilt in the cyanomet complex of oxygen-avid *Ascaris suum* hemoglobin, *J. Biol. Chem. 274*, 31819−31826.
48. Emerson, S. D., and La Mar, G. N. (1990) NMR determination of the orientation of the magnetic susceptibility tensor of cyano metmyoglobin: A new probe of steric tilt of bound ligand, *Biochemistry 29*, 1556−1566.
49. Lecomte, J. T. J., and La Mar, G. N. (1987) Proton NMR probe for hydrogen bonding of distal residues to bound ligands in heme proteins: isotope effect on heme electronic structure of myoglobin, *J. Am. Chem. Soc. 109*, 7219−7220.
50. Morishima, I., and Inubushi, T. (1978) ^{15}N nuclear magnetic resonance studies of iron-bound C^{15}N− in ferric low-spin cyanide complexes of various porphyrin derivatives and various hemoproteins, *J. Am. Chem. Soc. 100*, 3568−3574.
51. Behere, D. V., Gonzalez-Vergara, E., and Goff, H. M. (1985) Unique cyanide nitrogen-15 nuclear magnetic resonance chemical shift values for cyano-peroxidase complexes. Relevance to the heme-active site structure and mechanism or peroxide activation, *Biochim. Biophys. Acta 832*, 319−325.
52. Yamamoto, Y., and Suzuki, T. (1996) NMR study of the active site of shark met-cyano myoglobins, *Biochim. Biophys. Acta 1293*, 129−139.
53. Rivera, M., Seetharaman, R., Girdhar, D., Wirtz, M., Zhang, X., Wang, X., and White, S. (1998) The reduction potential of cytochrome b_5 is modulated by its exposed heme edge, *Biochemistry 37*, 1485−1494.
54. Cowley, A. B., Altuve, A., Kuchment, O., Terzyan, S., Zhang, X., Rivera, M., and Benson, D. R. (2002) Toward engineering the stability and hemin-binding properties of microsomal cytochromes b_5 into rat outer mitochondrial membrane cytochrome b_5: examining the influence of residues 25 and 71, *Biochemistry 41*, 11566−11581.
55. Hargrove, M. S., Brucker, E. A., Stec, B., Sarath, G., Arredondo-Peter, R., Klucas, R. V., Olson, J. S., and Phillips, G. N. (2000) Crystal structure of a nonsymbiotic plant hemoglobin, *Struct. Fold. Des. 8*, 1005−1014.
56. Milani, M., Ouellet, Y., Ouellet, H., Guertin, M., Boffi, A., Antonini, G., Bocedi, A., Mattu, M., Bolognesi, M., and Ascenzi, P. (2004) Cyanide binding to truncated hemoglobins: a crystallographic and kinetic study, *Biochemistry 43*, 5213−5221.
57. Dou, Y., Olson, J. S., Wilkinson, A. J., and Ikeda-Saito, M. (1996) Mechanism of hydrogen cyanide binding to myoglobin, *Biochemistry 35*, 7107−7113.
58. Mintorovitch, J., and Satterlee, J. D. (1988) Anomalously slow cyanide binding to *Glycera dibranchiata* monomer methemoglobin component II: implication for the equilibrium constant, *Biochemistry 27*, 8045−8050.
59. Du, W., Syvitski, R., Dewilde, S., Moens, L., and La Mar, G. N. (2003) Solution ^{1}H NMR characterization of equilibrium heme orientational disorder with functional consequences in mouse neuroglobin, *J. Am. Chem. Soc. 125*, 8080−8081.
60. Li, Y., Syvitski, R. T., Chu, G. C., Ikeda-Saito, M., and Mar, G. N. (2003) Solution ^{1}H NMR investigation of the active site molecular and electronic structures of substrate-bound, cyanide-inhibited HmuO, a bacterial heme oxygenase from *Corynebacterium diphtheriae*, *J. Biol. Chem. 278*, 6651−6663.
61. Friedman, J., Lad, L., Deshmukh, R., Li, H., Wilks, A., and Poulos, T. L. (2003) Crystal structures of the NO- and CO-bound heme oxygenase from *Neisseriae meningitidis*. Implications for O_2 activation, *J. Biol. Chem. 278*, 34654−34659.
62. Samuni, U., Ouellet, Y., Guertin, M., Friedman, J. M., and Yeh, S. R. (2004) The absence of proximal strain in the truncated hemoglobins from *Mycobacterium tuberculosis*, *J. Am. Chem. Soc. 126*, 2682−2683.
63. de Ropp, J. S., Sham, S., Asokan, A., Newmyer, S., Ortiz de Montellano, P. R., and La Mar, G. N. (2002) Influence of the distal his in imparting imidazolate character to the proximal his in heme peroxidase: ^{1}H NMR spectroscopic study of cyanide-inhibited His42→Ala horseradish peroxidase, *J. Am. Chem. Soc. 124*, 11029−11037.
64. Hargrove, M. S., Barrick, D., and Olson, J. S. (1996) The association rate constant for heme binding to globin is independent of protein structure, *Biochemistry 35*, 11293−11299.
65. Jue, T., Krishnamoorthi, R., and La Mar, G. N. (1983) Proton NMR study of the mechanism of the heme-apoprotein reaction for myoglobin, *J. Am. Chem. Soc. 105*, 5701−5703.
66. Pesce, A., Nardini, M., Ascenzi, P., Geuens, E., Dewilde, S., Moens, L., Bolognesi, M., Riggs, A. F., Hale, A., Deng, P., Nienhaus, G. U., Olson, J. S., and Nienhaus, K. (2004) ThrE11 regulates O_2 affinity in *Cerebratulus lacteus* mini-hemoglobin, *J. Biol. Chem. 279*, 33662−33672.
67. Kraulis, P. (1991) MOLSCRIPT: A program to produce both detailed and schematic plots of protein structures, *J. Appl. Crystallogr. 24*, 946−950.

BI048726L